



The contribution of archeometry in characterization of decorative materials from the site of *Villa di Teodorico* in Galeata (Italy)

Luciana Saviane¹, Maurizio Aceto^{2,3} , Laura Fornasini⁴ , Luciana Mantovani⁵ , Alessia Morigi¹, Riccardo Villicich¹, Danilo Bersani^{4,a} 

¹ Dipartimento di Discipline Umanistiche, Sociali e delle Imprese Culturali, Università degli Studi di Parma, Via M. D'Azeglio 85, 43125 Parma, Italy

² Dipartimento per lo Sviluppo Sostenibile e la Transizione Ecologica, Università degli studi del Piemonte Orientale, Piazza S. Eusebio, 5 - 13100 Vercelli, Italy

³ Centro Interdisciplinare per lo Studio e la Conservazione del Beni Culturali, Università degli Studi del Piemonte Orientale, Via Manzoni 8, 13100 Vercelli, Italy

⁴ Dipartimento di Scienze Matematiche, Fisiche e Informatiche, Università degli Studi di Parma, Parco Area delle Scienze 7/a, 43124 Parma, Italy

⁵ Dipartimento di Scienze Chimiche, della Vita e della Sostenibilità Ambientale, Università degli Studi di Parma, Parco Area delle Scienze 157/a, 43124 Parma, Italy

Received: 17 October 2022 / Accepted: 9 January 2023

© The Author(s) 2023

Abstract *Villa di Teodorico* in Galeata (Forlì-Cesena, Emilia Romagna) is an important archeological site in the north of Italy occupied from sixth century BC to twelfth century AD. The most interesting results concern the Roman age, when a large *villa* was built, and the late antiquity, when the Ostrogothic king Theodoric decided to build in this area his *palatium* (early sixth century AD). The archeometric investigation was performed on Roman wall paintings fragments and on late antique glass *sectilia* fragments belonging to *Palazzo di Teodorico* by using a multi-technique approach that included micro-Raman spectroscopy, scanning electron microscopy with energy-dispersive spectroscopy, X-ray powder diffraction, UV–visible–NIR diffuse reflectance spectrophotometry with optic fibers and optical stereo-microscopy. This analytical approach allowed the identification of all components, collecting molecular, elemental, microscopic, morphological and chromatic data. The characterization of samples supplied essential archeological, historical and technological information. The production techniques and the rich materials employed suggest the importance of the site in different periods. The evolution of the manufacturing technologies and the possible trade routes mainly during late antique period are witnessed by the change in the raw materials.

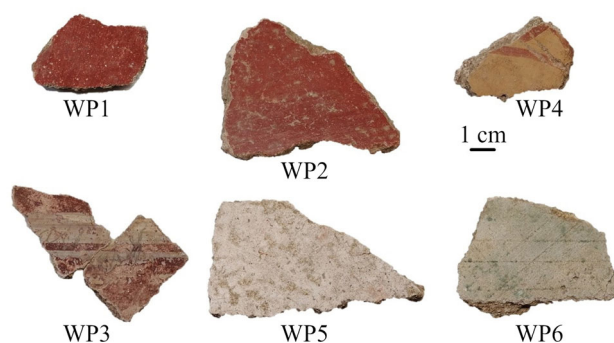
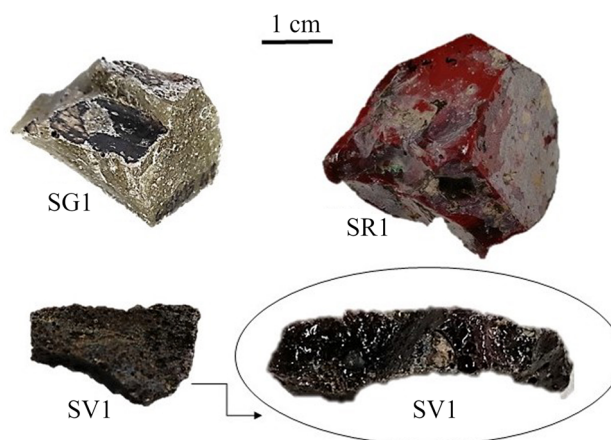
1 Introduction

The site of the *Villa di Teodorico* in Galeata (Forlì-Cesena, Emilia Romagna, Northern Italy) has given back a great variety of materials during archeological excavations [1–3]. It is a multi-layered site. The former presence of a country villa of republican age, with two kilns for the production of pottery, is documented [2, 3]. The most interesting phases concern the Roman age and the late antiquity when *Villa di Teodorico* was built (early sixth century AD) [1–5]. It was a pavilions villa: in the south-east, there is the thermal baths complex, while in the northern part there is the most prestigious sector with an octagonal room paved with an intact mosaic and neighboring rooms also paved with mosaics [1–3]. In particular in the polygonal room, a lot of glass mosaic *tesserae*, discovered in the collapse layers, suggest an inside decoration with wall mosaics [2–5]. The presence of a polygonal room, with different purposes, starts to spread in the residential architecture in late antiquity as a sign of prestige [1]. The composition of the main mosaic shows similarities with other famous ones present in the near city of Ravenna, as the “Domus dei Tappeti di Pietra” [1].

The characterization of finds is an important source of archeological, historical and technological information. The production techniques and the raw materials used can throw light on the importance of site in different periods and, mainly for late antique phase, on the evolution of the manufacturing technologies of that period and on the possible trade routes. The study of glass samples was challenging because they are composed by amorphous material, in which the network former compounds (mostly silica) were mixed with glass modifiers and flux agents. Moreover, the color of these materials was obtained in a lot of different ways: by means of micrometric coloring crystalline materials, using nanocrystalline colloids or dispersing transition metal ions in very small

Focus Point on Scientific Research in Cultural Heritage 2022 Guest editors: L. Bellot-Gurlet, D. Bersani, A.-S. Le Hô, D. Neff, L. Robinet, A. Tournié.

^a e-mail: danilo.bersani@unipr.it (corresponding author)

Fig. 1 Wall painting fragments investigated**Fig. 2** Glass *sectilia* fragments investigated and an inner detail of SV1

concentrations in the glassy matrix. Therefore, a multi-technique approach was required to know the nature of all components and to collect molecular, elemental, microscopic, morphological and chromatic information.

Some results have been already presented on several finds of this site, focused only one group of materials [4, 5].

This work reports the results of an archeometric investigation performed on Roman wall paintings fragments and glass *sectilia* fragments belonging to *Villa di Teodorico* by using an analytical approach that includes optical stereo-microscopy, micro-Raman spectroscopy [6–8], scanning electron microscopy with energy-dispersive spectroscopy (SEM-EDS) [9, 10], X-ray powder diffraction (XRPD) [11], UV–visible-NIR diffuse reflectance spectrophotometry with optic fibers (FORS) [12, 13]. Moreover, some additional data are reported about glass mosaic *tesserae* previously investigated [5].

2 Materials and methods

The sample set consists in 6 wall painting fragments and 3 glass *sectilia* fragments. Wall painting fragments are related to decoration of the *villa* during Roman age: two red, one yellow with red strips, one red with two white horizontal strips, one white and one green (Fig. 1). Glass finds were recovered during the last archeological excavations in the most prestigious sector of the *Villa di Teodorico*: tiles, previously investigated [5], decorated inner walls of the octagonal room and its vestibule [2, 3], while several glass *sectilia* fragments (Fig. 2) belonged probably to a floor in *opus sectile*: one red, one dark violet and one green-grayish. The *opus sectile* (cut work) is a wall or floor decoration composed on a resin and plaster support by inlaying flat marble, stone or glass slabs to make a picture or a pattern.

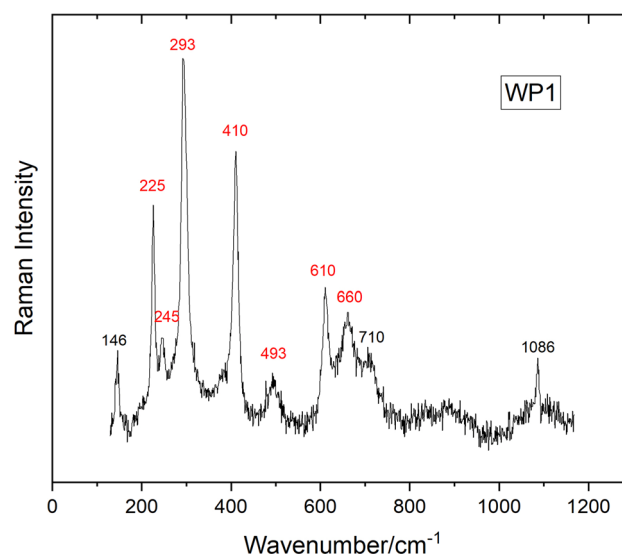
Each sample was preliminary observed using a stereo-microscope Optika, with 10–80 × magnification range, to get quickly first morphological information.

The crystalline phases were identified by means of micro-Raman analysis. Non-polarized Raman spectra were recorded at 632.8 nm (He–Ne laser) in a nearly backscattering geometry with a Horiba LabRam microspectrometer equipped with an integrated Olympus BX40 microscope. The spectral resolution was about 2 cm⁻¹. The power on the sample was kept under 10 mW using neutral density filters. A 50X ultra long working distance objective was used to collect the Raman signal. Micro-Raman maps were also performed on representative areas of the glass samples on linear or square matrix of points with stepsize of 4–5 μm. The acquisition time for each point was ranging from 20 to 30 s. False color images were obtained by associating the intensities of different colors to the intensities of characteristic vibrational modes of different compounds.

Textural observations and chemical analyses in different areas of fresh unaltered surfaces of the glass samples and on one wall painting fragment were performed using a JEOL 6400 scanning electron microscope (SEM), equipped with an Oxford-INCA energy

Table 1 Main compounds identified on the painted surface of samples

Sample	Color	Hematite	Calcite	Goethite	Green earths	Egyptian blue	Amorphous carbon	Gypsum
WP1	Red	X	X					
WP2	Dark red	X	X				X	
WP3	Red and white	X	X				X	
WP4	Yellow and red	X	X	X				
WP5	White		X					
WP6	Green		X		X	X		X

Fig. 3 Raman spectrum of red sample WP1 showing hematite (in red) and calcite (in black) peaks

dispersion X-Ray spectrometer (EDS). The operating conditions were accelerating voltage 20 kV and 1.2 mA current, $\sim 1 \mu\text{m}$ beam diameter and a counting time of 75 s.

The X-Ray powder diffraction (XRPD) patterns were collected from glass samples in order to determine the crystalline phases within the glassy matrix. The analyses were carried out on few milligrams of sample powder using a Bruker D2 phaser diffractometer, with Cu $K\alpha$ ($\lambda = 1.54178 \text{ \AA}$) radiation, 30 kV and 10 mA, Ni filtered, 2θ between 5 and 70° , steps of 0.02° and a sampling time of 1 s.

FORS was useful to identify and confirm the colorants of glass samples. FORS analyses were performed with an Avantes (Apeldoorn, The Netherlands), AvaSpec-ULS2048XL-USB2 model spectrophotometer and an AvaLight-DH-S-BAL balanced deuterium—halogen light source; the detector and the light source were connected to an FCR-7UV200-2– 1.5×100 probe by means of fiber-optic cables. The spot size on the sample was 2 mm.

3 Results and discussion

3.1 Pigments of wall painting fragments

The colors of samples are red (WP1), dark red (WP2), red and white (WP3), red and yellow (WP4), white (WP5), green (WP6). We studied all wall painting fragments through micro-Raman spectroscopy and one sample (WP6) also through SEM–EDS to obtain information on the pigments. Table 1 shows the compounds detected on the painted surfaces of samples.

The Raman analysis of the red fragments (WP1, WP2) and of the fragments with red background (WP3) and with red strips (WP4) proved the presence of hematite (Fe_2O_3) to make red color, with typical peaks (the main peaks are highlighted in bold type) at **225**, **245**, **293**, **410**, **493**, **610**, **660** cm^{-1} (Fig. 3). Hematite is the pigment present in red ochre [14]. The extra peak at 660 cm^{-1} was often attributed to magnetite because of a partial transformation of hematite into magnetite under the laser beam [6, 15]; instead, it is related to hematite herself and it is due to disorder and/or the presence of nanocrystals [16, 17].

Amorphous charcoal was detected for dark red of WP2 (Fig. 4) and WP3 by broad bands around 1350 and 1550 cm^{-1} ; in fact, amorphous carbon was often added to different pigments to create darker shades [14] or to obtain black pigments [18].

Fig. 4 Raman spectrum of amorphous carbon of dark red sample WP2

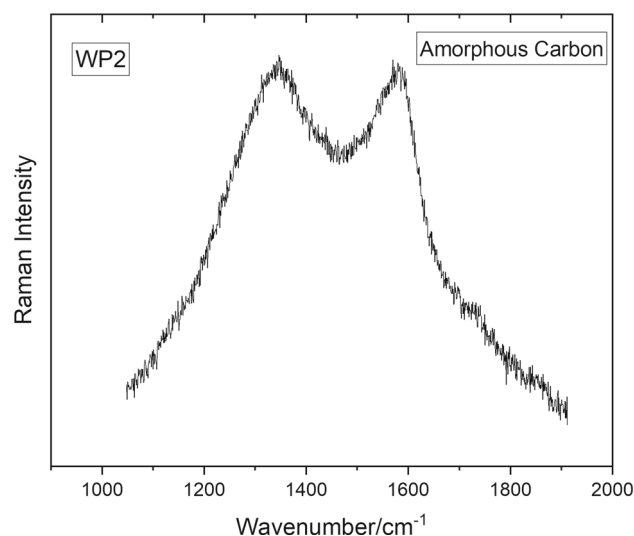
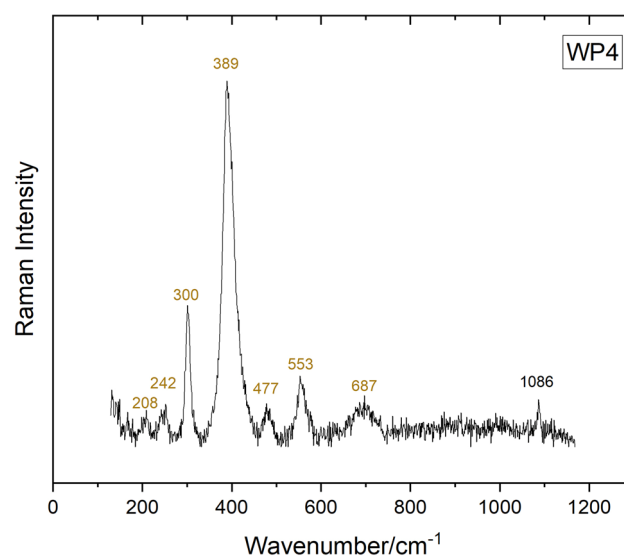


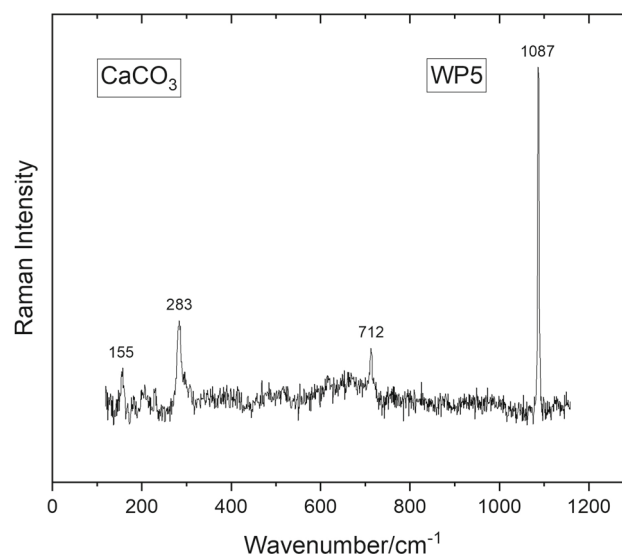
Fig. 5 Raman spectrum of red sample WP4 showing goethite (in yellow) and calcite (in black) peaks



In the sample WP4, the yellow color of background is mainly composed of goethite ($\text{Fe}^{3+}\text{O}(\text{OH})$), pigment present in yellow ochre, with peaks at 208, 242, **300**, **389**, 477, 553, 687 cm^{-1} (Fig. 5).

The white color of WP5 and of two strips of WP3 is due to calcite (CaCO_3) (Fig. 6), which was identified also in all samples (Figs. 3, 5) because of the carbonation of lime, used as a binder to embed the mineral pigment. So its presence is constant.

In the WP6 sample, the green color is conserved only in a few parts. The surface is almost white with millimeter-size greenish spots, containing micrometric blue crystals, not visible at naked eye. The green part is probably due to green earths: Raman spectra obtained from green crystals aren't clear, even if some of them can be compatible with green earths. EDS data (Table 2) suggest more clearly the use of green earths with the presence of magnesium, aluminum, silica, potassium and iron. It is difficult to distinguish the two main components of green earths, celadonite (approximately $\text{K}[(\text{Al}, \text{Fe}^{3+}), (\text{Fe}^{2+}, \text{Mg})] (\text{AlSi}_3, \text{Si}_4) \text{O}_{10} (\text{OH})_2$) or glauconite (approximately $(\text{K}, \text{Na}) (\text{Fe}^{3+}, \text{Al}, \text{Mg})_2 (\text{Si}, \text{Al})_4 \text{O}_{10} (\text{OH})_2$), because they are characterized by a similar chemical composition and similar Raman spectra. However, literature suggests that from the ratio $\text{Si}:\text{Al}:\text{Mg}$ it is possible to differentiate glauconite from celadonite [20]; in our case, the trend is $\text{Si} > \text{Al} > \text{Mg}$, so probably glauconite is present. The blue dots are composed by cuprorivaite ($\text{CaCuSi}_4\text{O}_{10}$), a calcium-copper tetrasilicate which is the main component of ancient Egyptian blue, the famous synthetic pigment added to green earths by Roman wall painters to achieve more brilliant colors [19]. SEM-EDS analysis shows the presence of silica, calcium and copper in the blue crystals (Fig. 7a-b). A Raman micro-map (8×8 point) was performed in a region of $40 \times 40 \mu\text{m}^2$ containing a cluster of well-defined blue crystals in order to better characterize them. The false-color Raman map reported in Fig. 7c confirms the presence of cuprorivaite in the blue crystals (blue color in the map, revealed by the main peaks at 433 and 110 cm^{-1} (Fig. 7d) surrounded by calcite (red color in the map) and gypsum, calcium sulfate bi-hydrate (green in the map, main peaks at 1005 and 412 cm^{-1}). Raman measurements reveal, in the same area, a minor presence of quartz (peak at 465 cm^{-1}) and possibly the presence of small amounts of the lead oxide litharge (main peak at 142 cm^{-1}).

Fig. 6 Raman spectrum of calcite of white sample WP5**Table 2** EDS data of sample WP6

Sample WP6	MgO	Al ₂ O ₃	SiO ₂	SO ₃	K ₂ O	CaO	Fe ₂ O ₃	CuO	ZnO
Blue crystals	n.d	n.d	65.44	n.d	n.d	14.6	n.d	19.55	0.4
Green surface	2.07	3.91	50.57	1.11	4.34	27.49	10.51	n.d	n.d

Data are expressed as weight percent, wt%. Abbreviation *n.d.* not detected)

Table 3 EDS data of glassy matrix of *sectilia* fragments

Sample	Color	SiO ₂	Al ₂ O ₃	MnO	MgO	CaO	Na ₂ O	K ₂ O	PbO	Fe ₂ O ₃	CuO	SnO ₂	Cl	SO ₃
SG1	Green-gray	68.2	2.3	1.9	1.0	8.2	15.5	0.7	n.d	0.7	n.d	n.d	1.0	0.5
SR1	Red	63.9	1.8	1.6	0.8	9.7	12.7	0.7	3.7	2.4	1.6	n.d	1.1	n.d
SV1	Dark violet	70.7	2.5	1.1	1.3	8.1	14	0.7	n.d	n.d	n.d	n.d	1.0	0.6

Data are expressed as weight percent, wt%. Abbreviation *n.d.* not detected)

3.2 Glass samples

3.2.1 Base glass composition

Different compositions of glassy matrix of *sectilia* fragments are provided in Table 3 and Fig. 8 in terms of major elements, expressed in oxides.

As mosaic glass *tesserae* [5], all samples analyzed show a soda-lime-silica glass composition, characterized by SiO₂ values ranging from 63.9 to 70.7 wt%, Na₂O from 12.7 to 15.5 wt%, MgO from 0.8 to 1.3 wt%, K₂O = 0.7 wt%.

The low contents of MgO and K₂O (< 1.5 wt%) indicate a natron source as flux (Fig. 8a), used in the Roman age until early Middle ages [21]. When their concentration surpasses the limit of 2.5 wt%, it is very likely that the glass was produced using plant ash as fluxing agent [22]. The high levels of Cl (ranging from 1 to 1.1 wt%) and SO₃ (ranging from 0.5 to 0.6 wt%) are related to natron that may contain NaCl and Na₂SO₄ as contaminants [10]. The CaO (from 8.1 to 9.7 wt%) and Al₂O₃ (from 1.8 to 2.5 wt%) amounts are constant (Fig. 8b), indicating the use of a common silica source containing feldspar as impurities [10].

Plots and models in literature about micro-Raman analysis of glassy silicate [23, 24] suggest important technological information. We considered, on the basis of the method used by Colomban et al. [24], the two main bands of silica glasses: one ascribed to Si–O bending, centered at about 500 cm⁻¹, and one relative to Si–O stretching, centered at about 1000 cm⁻¹. In Table 4, there are the values of Raman parameters extracted from one representative spectrum per sample: the position of the maxima δ_{\max} of the bending band, the position of the maximum ν_{\max} of the stretching band and the polymerization index I_p obtained as ratio between the intensities of the two bands (I_{500}/I_{1000}) [7, 25, 26]. The position of ν_{\max} ranges from 1095 to 1098 cm⁻¹, and the position of δ_{\max} Si–O ranges from 587 to 595 cm⁻¹. These data are compatible with values of a soda-lime-silicate glass. The values of the polymerization index I_p are between 0.87 and 0.94, typical of most Roman alkaline glasses ($0.8 < I_p < 1.1$) [24], confirming the results of SEM–EDS. Furthermore, polymerization index and wavenumber maxima of the Si–O bending and stretching are in agreement in the suggestion

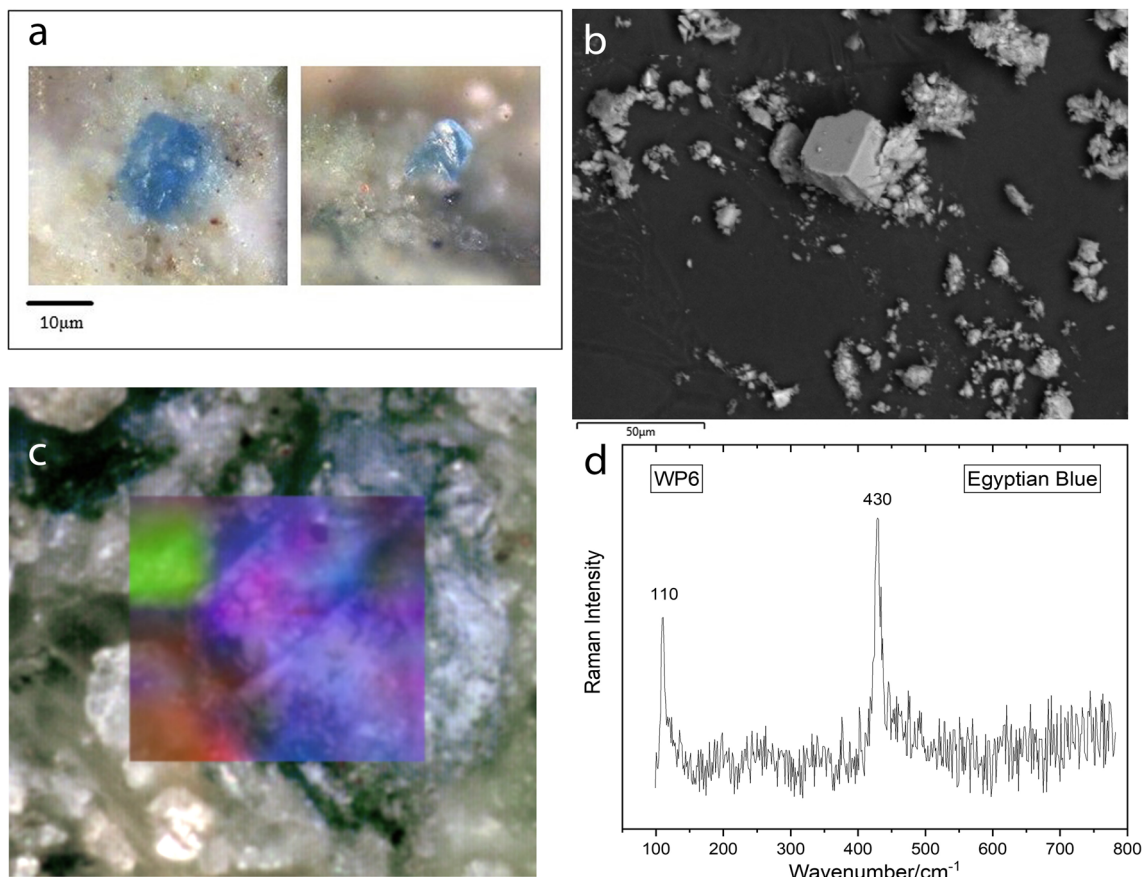


Fig. 7 (a) Microscope images of blue crystals of Egyptian blue of sample WP6; (b) BSE image of a blue crystal of Egyptian blue of sample WP6 (c) $40 \times 40 \mu\text{m}^2$ false color Raman map (8×8 points) of a region of WP6 sample. Blue = cuprorivaite (intensity of the peak at 430 cm^{-1}), red = calcite (1086 cm^{-1}), green = gypsum (1005 cm^{-1}); (d) Raman spectrum of Egyptian blue

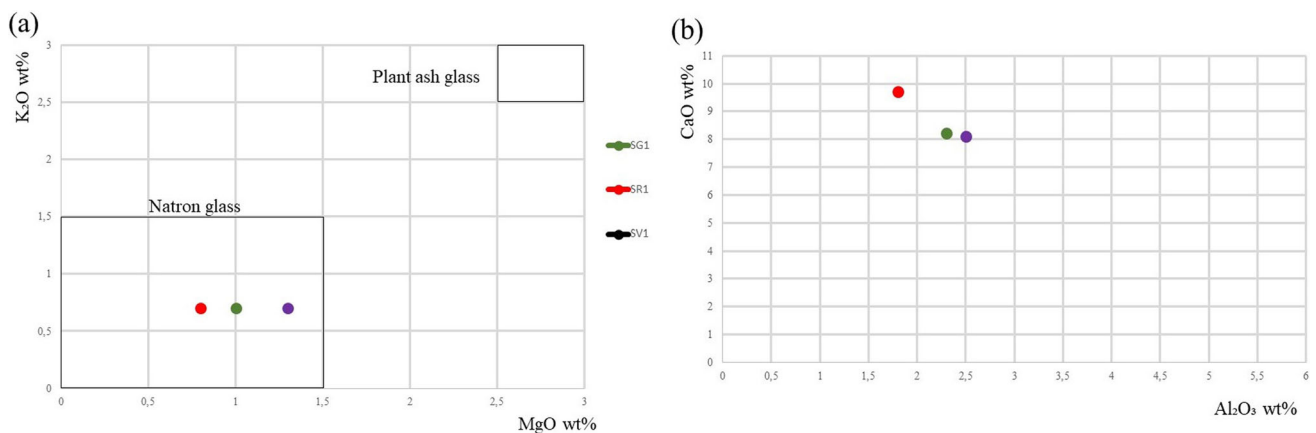


Fig. 8 Chemical composition of glass samples: (a) binary plot MgO versus K_2O ; (b) binary plot Al_2O_3 versus CaO

that the analyzed samples belong to the family of $\text{Na}_2\text{O} + \text{K}_2\text{O} + \text{CaO}$ glasses, as the comparison between Raman spectra and literature suggests [7, 26]. Finally, considering the empirical relationship between I_p and the firing temperature, we can suppose $T_f = \sim 1000 \text{ }^\circ\text{C}$ for $I_p \sim 1$ that corresponds to most ancient glasses [24].

3.2.2 Colorants and opacifiers

All *sectilia* fragments are intensively colored, and three groups of colors can be distinguished: red, violet and green. Opacification and, in some case, coloration are obtained by tiny (nano- to micrometric) crystalline phases embedded in the glassy matrix, identified

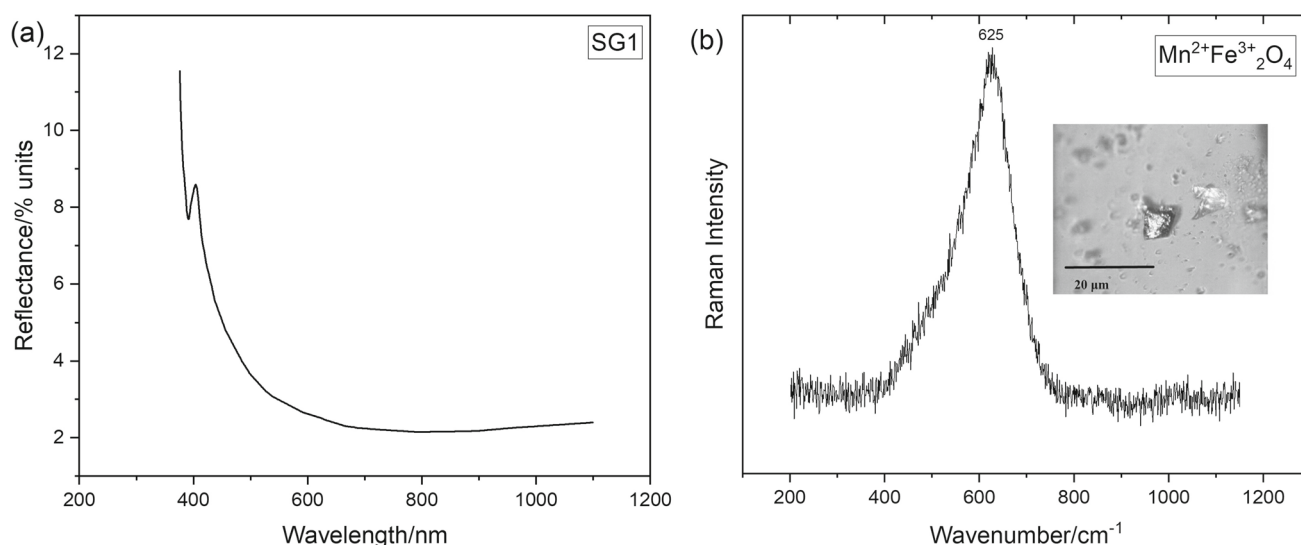
Table 4 Raman parameters extracted from spectra SG1, SR1, SV1

Sample	I_p	δ_{\max} Si–O	ν_{\max} Si–O
SG1	0.87	587	1098
SR1	0.94	590	1098
SV1	0.90	595	1095

Wavenumber positions in cm^{-1} **Table 5** Colorants and opacifiers for all differently colored *sectilia*

Sample	Color	Coloring agents	Opacifying agents
SG1	Green-grayish	$\text{Cu}^{2+} + \text{Mn}^{2+}\text{Fe}^{3+}_2\text{O}_4$	Ca-phosphate: hydroxyapatite ($\text{Ca}_5(\text{PO}_4)_3(\text{OH})$) and β -rhenanite ($\beta\text{-NaCaPO}_4$) + wollastonite (CaSiO_3)
SR1	Red	$\text{Cu}^0 + \text{Fe}_2\text{O}_3$	Cassiterite (SnO_2); Ca-phosphate: hydroxyapatite ($\text{Ca}_5(\text{PO}_4)_3(\text{OH})$) and β -rhenanite ($\beta\text{-NaCaPO}_4$)
SV1	Dark violet	Mn^{3+}	Ca-phosphate: hydroxyapatite ($\text{Ca}_5(\text{PO}_4)_3(\text{OH})$) and β -rhenanite ($\beta\text{-NaCaPO}_4$) + wollastonite (CaSiO_3)

Some compounds acting as both colorants and opacifiers are in the column of the main role

**Fig. 9** Analyses of *sectile* SG1: (a) FORS spectrum; (b) microscope image and Raman spectrum of a jacobsite inclusion

by micro-Raman spectroscopy. A lot of colors were produced by transition metal ions dispersed in the glassy matrix, requiring the help of SEM–EDS and FORS for their correct identification.

The results about coloring and opacifying agents are summarized in Table 5.

In the green-gray sample SG1, FORS analyses show a broad absorption band centered at about 800 nm due to Cu^{2+} (Fig. 9a), not revealed by EDS. The amount of copper required to color a glass is very small, in the range of 0.1 wt%, often under the detection limit of EDS equipments. EDS data show the presence of iron with in addition slightly elevated levels of manganese (1.87 wt% of MnO). These values ($\text{MnO} > 1$) suggest an intentional addition of manganese [22]. Concerning that point, interestingly Raman measurements directly performed on reddish crystals of SG1 demonstrated that they are consistent with the jacobsite ($\text{Mn}^{2+}\text{Fe}^{3+}_2\text{O}_4$) for the strong peak at 625 cm^{-1} (Fig. 9b). Jacobsite is a manganese iron oxide and maybe acts as coloring agent together with copper.

Calcium phosphate operates as opacifier, and its use was confirmed by the Raman spectra of some whitish inclusions (Fig. 10a) showing the signature of hydroxyapatite ($\text{Ca}_5(\text{PO}_4)_3(\text{OH})$) with bands located in the region between 430 and 1075 cm^{-1} (peaks at 430, 444, 580, 590, 608, **962**, 1026, 1046, 1075 cm^{-1}) (Fig. 10b) on the core of some crystals found in the glassy matrix [27, 28]. Interestingly on the border of the crystals, the signature of another phosphate was observed: β -rhenanite ($\beta\text{-NaCaPO}_4$) with bands located in the region between 429 and 1046 cm^{-1} (peaks at 429, 448, 582, **965**, 1012, 1024, 1046 cm^{-1}) (Fig. 10c) [27, 28]. In addition, the signature of wollastonite (CaSiO_3) (peaks at 413, 638, 889, **970 cm^{-1}) was detected surrounding some of the phosphate crystals [27, 28].**

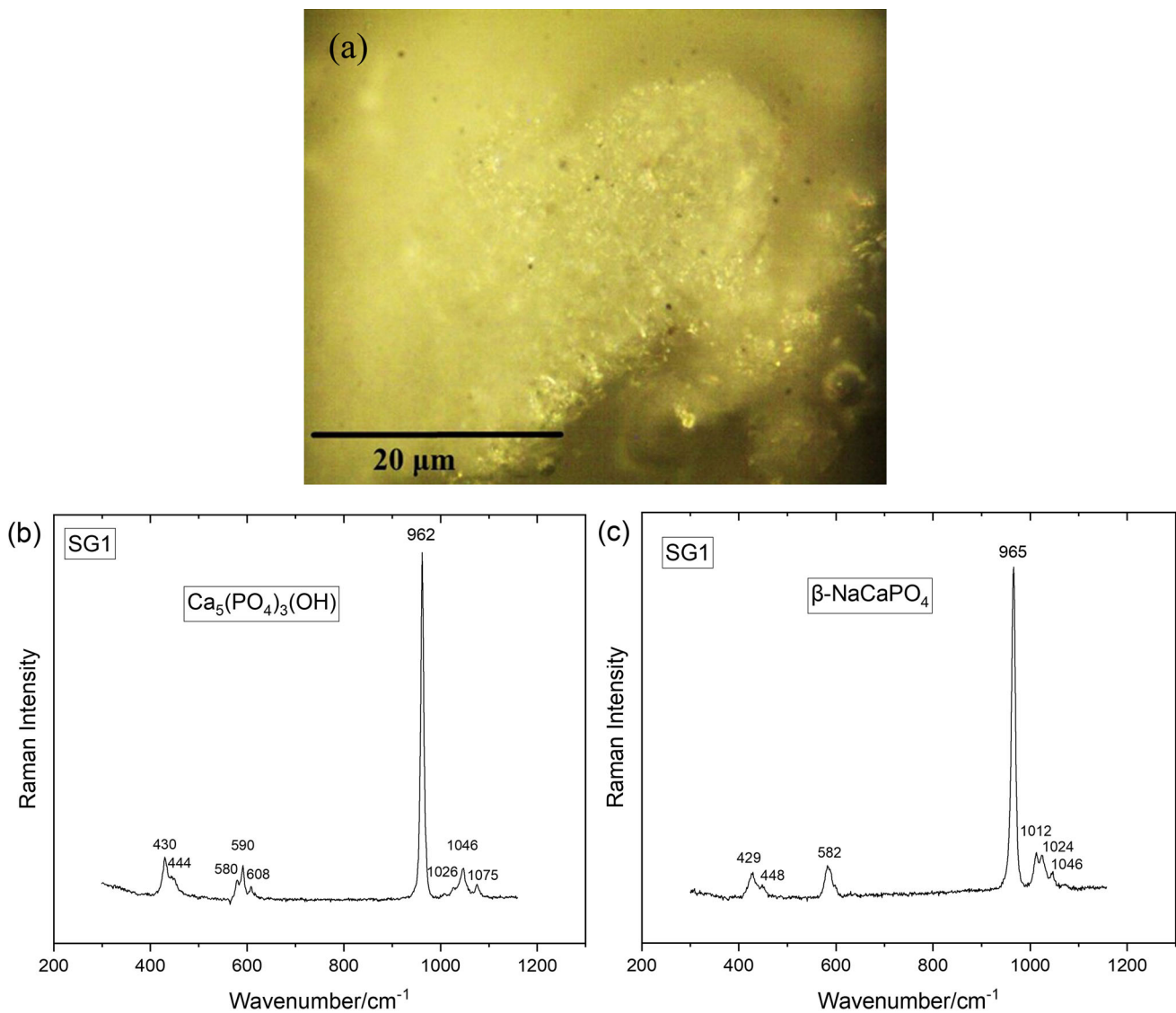


Fig. 10 Analyses of a Ca-phosphate inclusion in *sectile* SG1: (a) microscope image; (b) Raman spectrum of the core; (c) Raman spectrum of the border

β -Rhenanite and wollastonite are formed when crystals of apatite, belonging to bones used as raw material, react with the glassy matrix at about 650–700 °C [27–29]: in particular, the diffusion of sodium from glass to hydroxyapatite caused β -rhenanite and the diffusion of calcium from hydroxyapatite to glass caused the formation of wollastonite crystals near hydroxyapatite/ β -rhenanite particles [27]. The interaction of the phosphate crystals with the silicate glass was further investigated by micro-Raman mapping (Fig. 11a, b). A linear map was obtained on a whitish opacifier crystal, from its core to its external border (Fig. 11a). The inner part showed the signals of hydroxyapatite which were first replaced by those of β -rhenanite and then by those of wollastonite, moving outwards (Fig. 11c, d). Near the outer part of an opacifier crystal, the spatial distribution of these compounds was additionally highlighted by collecting a bidimensional map (Fig. 11b). The intensities of characteristic signals of β -rhenanite (ν_4 PO₄³⁻ bending modes between 560 and 610 cm⁻¹) and wollastonite (Si–O_{br} stretching mode at 638 cm⁻¹) were associated with the intensities of different colors (green and red, respectively) in the false color image (inset in Fig. 11b). It was noted that the layer of β -rhenanite was surrounded by that of wollastonite further outside.

Calcium phosphate is the main component of animal bones, which were crushed, powered, burnt and added to the translucent (colored) glass [27, 29, 30]. Some experimental replicas demonstrated that this opacification technique requires the addition of pre-fired bone to a base glass (excluding the use of unfired bone) and long melting temperature, from 18 to 36 h, with the formation of small and well-distributed gas bubble [28]. If the glass is exposed to a hot environment for over 36 h, compositional changes occurs, with the replacement of sodium with calcium, without a complete transformation into β -rhenanite and with the formation of a partially fused reaction rim of β -rhenanite [28]. It was noted that bigger inclusions usually show a reaction rim, while in smaller

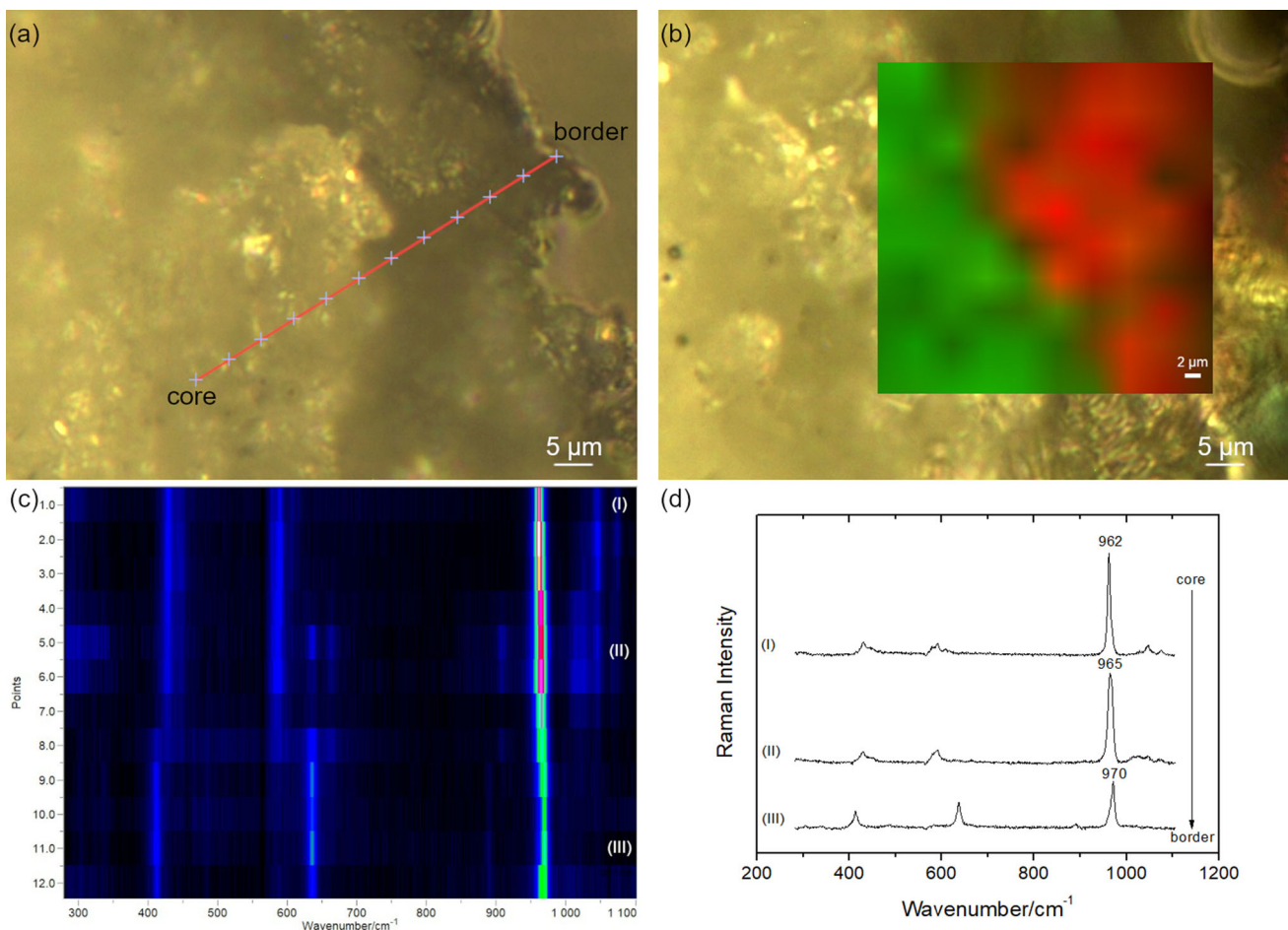


Fig. 11 (a) Microscope image of the opacifier crystal where the linear map (12×1) was performed; (b) microscope image of the opacifier crystal where the square map (10×10) was performed. In the inset, the false color image corresponding to the mapped area is reported. Green, β -rhenanite; red, wollastonite; (c) bidimensional visualization of the linear profile of Raman spectra obtained from the core to the border of the opacifier crystal (d) representative Raman spectra collected on the linear profile: (I) apatite, (II) β -rhenanite, (III) wollastonite

inclusions (approximately $100 \mu\text{m}$) the replacement of sodium with calcium takes place completely and there aren't reaction rims, tending to be more compact [27, 29].

Ca-phosphate was used from fifth-sixth century AD onwards, substituting Ca-antimonate and tin-based phases because probably they were more expensive and less accessible [27, 29]. Nevertheless, we haven't known exactly yet when and where this glass opacification technology was born and how it spread, but it is interesting that it was recognized in blue, turquoise and green glass from sites of Eastern Mediterranean, e. g. Turkey, Cyprus, Jordan, Palestine, but also Padua and Ravenna in Italy [29, 30].

FORS analyses, with an inflection point at about 590 nm , indicated that the red color of SR1 is due to metallic copper Cu^0 (Fig. 12a), present as suspension of submicrometric colloidal particles. XRPD didn't confirm this information (Fig. 12b), probably due to the overall low amount of copper particles, conversely to orange (O1) and red *tesserae* (R1, R2, R3) which were previously investigated [5]: indeed, the pattern doesn't present the typical peaks of metallic copper, because probably it is in a low amount, under the detection limit of the used XRPD. Moreover, FORS spectrum shows an absorption band at about 1100 nm attributable to ion Fe^{2+} (Fig. 12a) and SEM-EDS demonstrated relevant iron values (Fe_2O_3 2.4 wt%); hence, in this case the role of reducing agent was played by iron. In fact, the formation of red color required a reducing atmosphere in the furnace to obtain the reduction from Cu^{2+} to Cu^{1+} for cuprite or Cu^0 for metallic copper [13, 22, 29, 31] and reducing agents could be iron, tin, antimony [13, 31] but also charcoal or furnace ash [29, 31].

Two main types of manufacturing technology of opaque red glass were attested: "sealing wax red glass," a bright glass with high lead and copper contents and dendritic crystals of cuprite (Cu_2O) [13, 29], mostly documented from fourth century BC to first century AD [13], and "dullish red glass" [29] called also "red brown glass" [13] or "low-lead and low-copper red glass" [7], characterized by low lead ($\text{PbO} < 15 \text{ wt\%}$) and copper (CuO 1–5 wt%) contents, the addition of iron (Fe_2O_3 1–4 wt%) [7, 13] and nanometric particles of metallic copper dispersed into the vitreous matrix [29]. The last one is documented after first century AD until present day; it is a cheaper technology with fewer metals employed and less time of production, because the formation

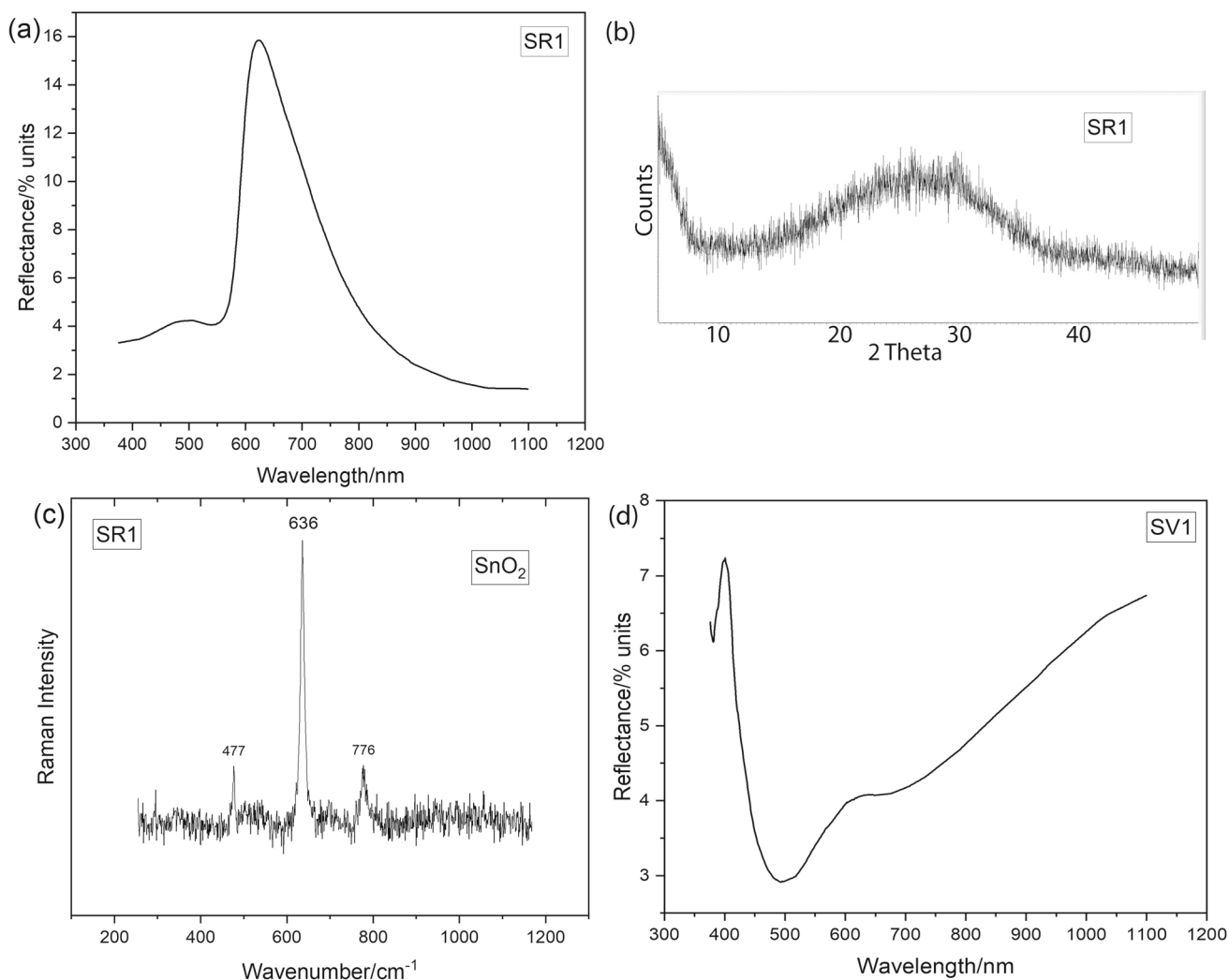


Fig. 12 Analyses of *sectilia* SR1 and SV1: (a) FORS spectrum of SR1; (b) XRPD pattern from SR1; (c) Raman spectrum of cassiterite in SR1; (d) FORS spectrum of SV1

of cuprite crystals of the first type required a long heat treatment, while the precipitation of metallic particles of the second type happened during the cooling phase [13]. However, there aren't important visual differences among the two categories and several red hues are included under the designation “red brown” [13]. In the sample SR1, whose color is due to metallic copper, SEM–EDS data display low levels of copper (CuO 1.6 wt%) and lead (PbO 3.7 wt%) and values of iron in the range 1–4 wt% [13] (Fe_2O_3 2.4 wt%); therefore, it is ascribable to “red brown glass”.

Metallic copper acts as colorant but also as opacifier together with cassiterite (SnO_2) and calcium phosphate, identified by micro-Raman spectroscopy. In fact, Raman spectra of some whitish inclusions are characterized by typical peaks of cassiterite at 477, 636 and 776 cm^{-1} (Fig. 12c), whereas micro-Raman measurement carried out on other inclusions highlighted different compositional features on the core and the border: the spectrum of the core is consistent with hydroxyapatite ($\text{Ca}_5(\text{PO}_4)_3(\text{OH})$), with bands located in the region between 430 and 1075 cm^{-1} , and the spectrum of the border is consistent with β -rhenanite ($\beta\text{-NaCaPO}_4$), with bands located in the region between 429 and 1046 cm^{-1} .

Comparing this sample with three red glass *tesserae* of the same site and the same period [5], it is interesting to observe that also tiles belong to the “dullish red glass” category, even if lead is slightly higher (PbO between 5.2 and 7 wt%) and a sample (R2) is very rich in copper (CuO 9.8 wt%) [5], suggesting a different production technology for this *tessera*. Metallic copper is responsible of red color of tiles and also acts as opacifier together with only cassiterite [5].

Hence, all our red samples don't contain antimony-based crystalline phases (calcium and lead antimonate), which were the main opacifying agents during the Roman age. They were substituted progressively by tin-based phases from fourth century AD [5, 31], perhaps because of either the interruption in the supply of antimony or the beginning of closer relations between the Roma Empire and India [5, 29, 32, 33], and by calcium phosphate.

The dark violet hue of SV1 was obtained using manganese: in fact, FORS technique detected ion Mn^{3+} as colorant, with an absorption maximum at 495 nm (Fig. 12d), and SEM–EDS analyses identified relevant values of manganese (MnO 1.1 wt%). The use of manganese as colorant, imparting a pink/purple color, is attested throughout the history of glass production, from the Bronze Age until the Modern Age [34]. Moreover, manganese can also act as decoloring agent and its use with this role increased from fourth century AD until the Middle Ages, when it became the only one used [34].

Micro-Raman spectroscopy recognized Ca-phosphate as opacifier, also in this sample; in particular, Raman spectra acquired on the core and the rim of the inclusions show the typical peaks assigned, respectively, to hydroxyapatite ($\text{Ca}_5(\text{PO}_4)_3(\text{OH})$) and β -rhenanite ($\beta\text{-NaCaPO}_4$), but also the formation of wollastonite crystals (CaSiO_3) was demonstrated near the surface of hydroxyapatite/ β -rhenanite particles.

Finally, to complete the study of mosaic glass tiles [5], SEM–EDS and Raman data allowed some additional observations about antimony-based opacifiers (Ca-antimonate and Pb-antimonate). In blue and white samples both calcium antimonates, the hexagonal phase (CaSb_2O_6) and the cubic phase (CaSb_2O_7) were detected [5]. Two methods of production are supposed for Ca-antimonates: in situ crystallization process, obtained by adding antimony to the molten glass, and the “corpo” method, when the pigments are synthesized ex situ [31]. Some researches demonstrated that, for the in situ crystallization, the presence of two calcium antimonates, CaSb_2O_6 and CaSb_2O_7 , in the same sample, with a prevalence of the hexagonal one, seems to suggest a firing time of 1–2 days and a temperature of about 1100 °C, while the presence of only the hexagonal phase could indicate shorter firing times and a temperature over 1100 °C [22, 29, 31, 35, 36]. In our case, BSE images show a microstructure characterized by a relatively homogeneous distribution of crystals into glassy matrix [5]; this is a strong indicator of an in situ crystallization, which was obtained by adding antimony to the molten glass as stibnite in the raw form (Sb_2S_3) or as roasted stibnite (Sb_2O_3 or Sb_2O_4) [35, 36]. This information and the presence of both the hexagonal and cubic phases confirm a duration of heat treatment between 1 and 2 days at approximately 1100 °C [5, 31].

Instead, regarding bindheimite ($\text{Pb}_2\text{Sb}_2\text{O}_7$) used in the pink *tessera* P1 as coloring and opacifying agent [5], it is commonly accepted in the literature that Sb-antimonate was synthesized ex situ and then added to the molten glass in a very quick process [31]. This production method is consistent with the uneven distribution of crystals [31] observed by means of SEM [5].

4 Conclusions

Archeometric investigation on wall paintings pigments and on glassy matrix, coloring and opacifying agents of mosaic tiles from *Villa di Teodorico* in Galeata was carried out by a multi-technique approach.

The set of wall painting fragments is characterized by the presence of typical pigments used during the Roman age. In fact, hematite (Fe_2O_3) is responsible for red color, with the addition of amorphous carbon for a darker hue; yellow color is due to goethite ($\text{Fe}^{+3}\text{O}(\text{OH})$) and white color is due to calcite (CaCO_3), which was identified also in all samples because of the carbonation of lime, used as a binder to fix the mineral pigment. The green hue was obtained by green earths, perhaps glauconite, and by cuprorivaite ($\text{CaCuSi}_4\text{O}_{10}$), which is the main component of the famous Egyptian blue.

The set of samples concerning the late antique phase is made of soda-lime-silica glass, with natron as a flux (MgO and $\text{K}_2\text{O} < 1.5$ wt%) and calcium and aluminum in constant quantity.

Polymerization index obtained by Raman spectra suggests a processing temperature of about 1000 °C. Color and opacity of glass are due to chromophore ions and/or opacifying/coloring crystals. In the green-grayish *sectile* fragment, copper and jacobsite ($\text{Mn}^{2+}\text{Fe}^{3+}_2\text{O}_4$) act as colorant, while Ca-phosphate operates as opacifier. In particular, the Raman spectra of rim and core of calcium phosphate inclusions were consistent, respectively, with β -rhenanite ($\beta\text{-NaCaPO}_4$) and hydroxyapatite ($\text{Ca}_5(\text{PO}_4)_3(\text{OH})$), because of reactions between hydroxyapatite, belonging to bones used as raw material, and silica soda-lime glassy matrix of *sectilia*. As a product of this interaction, wollastonite (CaSiO_3) was also detected. Red hue was obtained by metallic copper, together with cassiterite (SnO_2) and Ca-phosphate. Moreover, low levels of copper and lead suggest that it belongs to type of “red brown glass”. Ca-phosphate is also employed in dark violet sample, colored by means of manganese.

Concerning some *tesserae* early investigated, Raman results permit some supplementary considerations about antimony-based opacifiers, common during the Imperial Age and replaced gradually by tin-based, lead–tin-based and calcium phosphate phases from the late antiquity. In blue and white tiles, a relatively homogeneous distribution of crystals into vitreous matrix indicates an in situ crystallization, which together with the presence of two Ca-antimonates, CaSb_2O_6 and CaSb_2O_7 , in the same sample, with a prevalence of the hexagonal one, confirms a firing time of 1–2 days and a temperature of about 1100 °C. In pink *tessera* Pb-antimonate ($\text{Pb}_2\text{Sb}_2\text{O}_7$) is distributed in non-homogeneous textures, suggesting the “corpo” method.

Acknowledgements The archeological excavations were supported, inside S.F.E.R.A. (Spazi e Forme dell’Emilia Romagna Antica) Program and Framework Agreement between Università di Parma and Comune di Galeata, by Archeological Mission at Villa di Teodorico in Galeata, led by Università di Parma (director Alessia Morigi, scientific managers Alessia Morigi and Riccardo Villicich) in MiC (Ministry of culture) concession.

Funding Open access funding provided by Università degli Studi di Parma within the CRUI-CARE Agreement.

Data Availability Statement This manuscript has associated data in a data repository. [Authors' comment: Data will be made available on reasonable request.]

Open Access This article is licensed under a Creative Commons Attribution 4.0 International License, which permits use, sharing, adaptation, distribution and reproduction in any medium or format, as long as you give appropriate credit to the original author(s) and the source, provide a link to the Creative Commons licence, and indicate if changes were made. The images or other third party material in this article are included in the article's Creative Commons licence, unless indicated otherwise in a credit line to the material. If material is not included in the article's Creative Commons licence and your intended use is not permitted by statutory regulation or exceeds the permitted use, you will need to obtain permission directly from the copyright holder. To view a copy of this licence, visit <http://creativecommons.org/licenses/by/4.0/>.

References

1. L. Saviane, Gli ambienti ottagonali della villa di Teoderico a Galeata e nell'architettura residenziale tardoantica. Degree Thesis (Università di Parma, 2017/2018)
2. A. Morigi, R. Villicich, Nuove ricerche archeologiche presso la Villa di Teoderico, The Journal of Fasti Online (2020) <http://www.fastionline.org/docs/FOLDER-it-2020-466.pdf>. Accessed 31 Aug 2022
3. A. Morigi, R. Villicich, in *Abitare nel Mediterraneo tardoantico. Atti del III Convegno Internazionale del Centro Interuniversitario di Studi sull'Edilizia abitativa tardoantica nel Mediterraneo (Bologna 28–31 ottobre 2019)*, ed. by I. Baldini, C. Sfamini (Edipuglia, Bari, 2021), pp.243–252
4. L. Saviane, A. Morigi, R. Villicich, L. Mantovani, M. Aceto, L. Fornasini, D. Bersani, Stud. Romagnoli **71**, 219 (2020)
5. D. Bersani, L. Saviane, A. Morigi, L. Mantovani, M. Aceto, L. Fornasini, J. Raman Spectrosc. (2021). <https://doi.org/10.1002/jrs.6180>
6. P. Baraldi, C. Baraldi, R. Curina, L. Tassi, P. Zannini, Vib. Spectrosc. (2006). <https://doi.org/10.1016/j.vibspec.2006.04.029>
7. P. Ricciardi, P. Colomban, A. Tournié, M. Macchiarola, N. Ayed, J. Archeol. Sci. (2009). <https://doi.org/10.1016/j.jas.2009.07.008>
8. E. Basso, C. Invernizzi, M. Malagodi, M.F. La Russa, D. Bersani, P.P. Lottici, J. Raman Spectrosc. (2014). <https://doi.org/10.1002/jrs.4449>
9. A. Conventi, E. Neri, M. Verità, Mat. Sci. Eng. (2012). <https://doi.org/10.1088/1757-899X/32/1/012007>
10. D. Barca, E. Basso, D. Bersani, G. Galli, C. Invernizzi, M.F. La Russa, P.P. Lottici, M. Malagodi, S.A. Ruffolo, Microchem. J. (2016). <https://doi.org/10.1016/j.microc.2015.10.037>
11. N. Schibille, C. Boschetti, M.A. Valero Tévar, E. Veron, J. De Juan Ares, Miner. (2020). <https://doi.org/10.3390/min10030272>
12. M. Aceto, G. Fenoglio, M. Labate, M. Picollo, M. Bacci, A. Agostino, J. Cult. Herit. (2020). <https://doi.org/10.1016/j.culher.2020.05.003>
13. M. Bandiera, M. Verità, P. Lehuédé, M. Vilarigues, Miner. (2020). <https://doi.org/10.3390/min10100875>
14. D. Miriello, A. Bloise, G.M. Crisci, R. De Luca, B. De Nigris, A. Martellone, M. Osanna, R. Pace, A. Pecci, N. Ruggieri, Miner. (2018). <https://doi.org/10.3390/min8040134>
15. M. Bouchard, D.C. Smith, Spectrochim. Acta Part A (2003). [https://doi.org/10.1016/S1386-1425\(03\)00069-6](https://doi.org/10.1016/S1386-1425(03)00069-6)
16. D. Bersani, P.P. Lottici, A. Montenero, J. Raman Spectrosc. (1999). [https://doi.org/10.1002/\(SICI\)1097-4555\(199905\)30:5%3c355::AID-JRS398%3e3.0.CO;2-C](https://doi.org/10.1002/(SICI)1097-4555(199905)30:5%3c355::AID-JRS398%3e3.0.CO;2-C)
17. C.M. Marshall, W.J.B. Dufresne, C.J. Ruffledt, J. Raman Spectrosc. (2020). <https://doi.org/10.1002/jrs.5824>
18. M.C. Caggiani, A. Cosentino, A. Mangone, Microchem. J. (2006). <https://doi.org/10.1016/j.microc.2016.06.020>
19. I. Aliatis, D. Bersani, E. Campani, A. Casoli, P.P. Lottici, S. Mantovani, I.-G. Marino, F. Ospitali, Spectrochim. Acta Part A (2009). <https://doi.org/10.1016/j.saa.2008.11.009>
20. F. Ospitali, D. Bersani, G. Di Leonardo, P.P. Lottici, J. Raman Spectrosc. (2008). <https://doi.org/10.1002/jrs.1983>
21. A. Silvestri, G. Molin, G. Salviulo, Archaeom. (2005). <https://doi.org/10.1111/j.1475-4754.2005.00233.x>
22. N. Schibille, P. Degryse, M. Corremans, C.G. Specht, J. Archaeol. Sci. (2012). <https://doi.org/10.1016/j.jas.2012.01.020>
23. P. Colomban, M.P. Etchevery, M. Asquier, M. Bounichou, A. Tournié, J. Raman Spectrosc. (2006). <https://doi.org/10.1002/jrs.1495>
24. P. Colomban, A. Tournié, L. Bellot-Gurlet, J. Raman Spectrosc. (2006). <https://doi.org/10.1002/jrs.1515>
25. P. Colomban, J. Non-Cryst. Solids (2003). [https://doi.org/10.1016/S0022-3093\(03\)00303-X](https://doi.org/10.1016/S0022-3093(03)00303-X)
26. P. Colomban, J. Cult. Herit. (2008). <https://doi.org/10.1016/j.culher.2008.06.005>
27. A. Silvestri, F. Nestola, L. Peruzzo, Microchem. J. (2016). <https://doi.org/10.1016/j.microc.2015.10.026>
28. S. Maltoni, A. Silvestri, J. Cult. Herit. (2019). <https://doi.org/10.1016/j.culher.2019.02.015>
29. M. Vandini, S. Fiorentino, Miner. (2020). <https://doi.org/10.3390/min10070609>
30. S. Fiorentino, T. Chinni, M. Vandini, J. Cult. Herit. (2020). <https://doi.org/10.1016/j.culher.2020.06.003>
31. S. Maltoni, A. Silvestri, Miner. (2018). <https://doi.org/10.3390/min8060255>
32. M. Tite, T. Pradell, A. Shortland, Archaeom. (2008). <https://doi.org/10.1111/j.1475-4754.2007.00339.x>
33. E. Neri, C. Morvan, P. Colomban, M. F. Guerra, V. Prigent, Ceram. Int. (2016). <https://doi.org/10.1016/j.ceramint.2016.09.033>
34. A. Silvestri, F. Nestola, L. Peruzzo, Miner. (2020). <https://doi.org/10.3390/min10100881>
35. S. Lahlil, I. Biron, L. Galois, G. Morin, Appl. Phys. A Mater. Sci. Process. (2008). <https://doi.org/10.1007/s00339-008-4456-8>
36. S. Lahlil, I. Biron, M. Cotte, J. Susini, Appl. Phys. A Mater. Sci. Process. (2010). <https://doi.org/10.1007/s00339-010-5650-z>